AAS 22-630

LONG-TERM CISLUNAR SURVEILLANCE VIA MULTI-BODY RESONANT TRAJECTORIES

Maaninee Gupta[*], Kathleen C. Howell[†], and Carolin Frueh[‡]

In the coming decades, numerous spacecraft are expected to populate cislunar space, reaching beyond GEO and out to the lunar vicinity. The complex cislunar dynamical environment necessitates the use of new and unique orbits for sustaining long-term operations and surveillance. In this investigation, resonant orbits are incorporated into the trajectory design process to expand the range of cislunar trajectories as options for space domain awareness. The properties of the proposed itineraries facilitate their long-term viability, which is validated in a higher-fidelity ephemeris model. Constellations of spacecraft in resonant orbits offer a promising catalog of trajectories for space-based sensors.

Over the past few decades, humanity has maintained a constant and sizable presence in the near-Earth orbital realm. Naturally, in pushing the technological and scientific boundaries, cislunar space is poised to become the next step for a sustained human presence in space. Specifically, the region extending outward from geosynchronous orbit (GEO) towards the lunar vicinity and the Earth-Moon L_1 and L_2 libration points is of particular interest.[1] With this expansion, it is necessary to acknowledge the vastness of cislunar space, yet also capture the significant subspaces to support and maintain any cislunar operations in the future. The increased number of commercial and military assets beyond GEO also necessitates regulation and constant monitoring, similar to the Space Domain Awareness (SDA) and Space Situational Awareness (SSA) architectures currently in place in the sub-GEO regime.

The United States Air Force (USAF) and the United States Space Force (USSF) are working to improve their cislunar monitoring capabilities.[2] The Cislunar Highway Patrol System (CHPS) was recently proposed by the Air Force Research Laboratory (AFRL), to provide active detection and tracking of cislunar objects.[3] Through CHPS, the USSF aims to significantly increase the scope of the SDA capabilities, extending beyond the lunar orbit. However, a major challenge inherent to operating spacecraft in cislunar space is the non-negligible gravitational influence of the Moon and the Sun. The resulting complex dynamical environment is not sufficiently modeled by Earth (or Moon) Keplerian motion. As such, a three-body dynamical model better reflects the complex behavior of trajectories in cislunar space.

This investigation extends the previous work by Frueh et al.[4,5] and Gupta et al.[6] in the exploration of cislunar surveillance orbits for SDA applications. The proposed trajectories span the near-Earth

[*]Ph.D. Student, School of Aeronautics and Astronautics, Purdue University, West Lafayette, IN 47906; gupta208@purdue.edu

[†]Hsu Lo Distinguished Professor of Aeronautics and Astronautics, School of Aeronautics and Astronautics, Purdue University, West Lafayette, IN 47907; howell@purdue.edu

[‡]Associate Professor, School of Aeronautics and Astronautics, Purdue University, West Lafayette, IN 47907; cfrueh@purdue.edu

vicinity (GEO belt) to the lunar orbit, providing direct line-of-sight from the spacecraft to the lunar far-side as well. The proposed rapid and repeated access between GEO and the L_1-Moon-L_2 region reduces the volume of space for surveillance and operational purposes, yielding itineraries that assist in cislunar SDA. These Earth-Moon "traffic lanes" provide direct access between the two bodies, while also yielding opportunities for excursions to other cislunar regions of interest.

The dynamical model in the Earth-Moon Circular Restricted Three-Body Problem (CR3BP) is employed in this investigation to adequately represent the cislunar dynamical environment. Resonant orbits, i.e., orbits in resonance with the orbit of the Moon, with naturally repeating behavior to survey cislunar space, provide an attractive option. The long-term behavior of spacecraft in the various proposed itineraries is also evaluated in the higher-fidelity ephemeris model, incorporating the gravitational perturbations from additional celestial bodies. Spacecraft constellations are examined to assess their value for observations. The sample proposed constellation is comprised of spacecraft that maintain their resonance with the period of the Moon and, consequently, naturally remain in a relative configuration. Additionally, localized access to the lunar vicinity is explored by leveraging Poincaré maps, revealing various homoclinic connections and the associated periodic orbits nearby the libration points. Options for transfers between the retrograde and prograde resonant orbits are also demonstrated. Finally, as a comparison, free return trajectories in the Earth-Moon system are computed in the CR3BP dynamical model. Their transit times and energy levels are assessed against the proposed resonant orbits.

DYNAMICAL MODELS

This investigation leverages two dynamical models for the computation and analysis of the proposed orbits. The first model is the Circular Restricted Three-Body Problem (CR3BP), that is employed in the computation of relevant baseline orbits. Further analysis of the orbits in a higher-fidelity dynamical environment is then delivered via the N-body ephemeris model, incorporating the additional gravitational perturbations due to the Sun and Jupiter.

Circular Restricted Three-Body Problem

The CR3BP is an autonomous dynamical model that incorporates the gravitational influences of two planetary bodies that can be a planet-moon or a Sun-planet pair. The Earth and the Moon produce the greatest levels of acceleration on spacecraft traversing the cislunar region and, thus, these are the two bodies that comprise the model in this analysis.[4] The Earth and the Moon, termed the primaries and denoted as P_1 and P_2, respectively, are assumed to be point masses orbiting their mutual barycenter in circular orbits. The third body represents a smaller body of infinitesimal mass relative to the masses of the primaries and is denoted as P_3. The CR3BP allows the motion of the third body, the spacecraft, to be modeled under the influence of P_1 and P_2. A rotating frame based in the motion of the primaries is adopted to describe the behavior of the spacecraft governed by the two bodies. This rotating frame moves at a constant rate, $\dot{\theta}$, relative to an inertial frame, and this rate is equal to the mean motion of the system. Figure 1 represents the orientation of the rotating reference frame, denoted $\hat{x}$-$\hat{y}$-$\hat{z}$, relative to the inertial reference frame, denoted $\hat{X}$-$\hat{Y}$-$\hat{Z}$, with both frames centered on the system barycenter, B, where the vector bases are dextral, orthonormal triads. Carets identify vectors of unit length.

The quantities l^*, m^*, and t^*, termed the characteristic length, characteristic mass, and characteristic time, respectively, are introduced to nondimensionalize the equations of motion in the CR3BP. The characteristic length is equal to the constant distance between the primaries, the characteristic

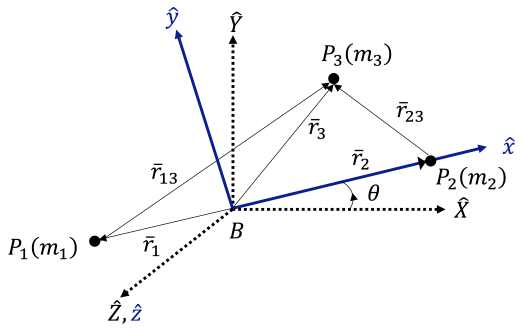

Figure 1. Schematic of the CR3BP inertial and rotating frames.

mass is equal to the sum of the masses of the primaries and, finally, the characteristic time is computed such that the nondimensional gravitational constant, $\tilde{G}$, is equal to unity. The nondimensional equations of motion that represent the motion of P_3 as expressed in the P_1-P_2 rotating frame are, thus, represented as,

$$\ddot{x} - 2\dot{y} = \frac{\partial U^*}{\partial x}, \quad \ddot{y} + 2\dot{x} = \frac{\partial U^*}{\partial y}, \quad \ddot{z} = \frac{\partial U^*}{\partial z} \tag{1}$$

The quantity U^* is the pseudo-potential function, expressed as,

$$U^* = \frac{1-\mu}{r_{13}} + \frac{\mu}{r_{23}} + \frac{x^2+y^2}{2} \tag{2}$$

where μ is the system mass parameter evaluated as $\mu = \frac{m_2}{m_1+m_2}$, and is roughly equal to 0.01215 for the Earth-Moon system. Additionally, r_{13} and r_{23} denote the nondimensional distances between the Earth and the spacecraft as well as the Moon and the spacecraft, respectively. The coordinates (x, y, z) correspond to the nondimensional position of the spacecraft relative to the system barycenter in the Earth-Moon rotating frame; similarly, $(\dot{x}, \dot{y}, \dot{z})$ represents the velocity components of the spacecraft as viewed in the rotating frame. Five equilibrium solutions that are termed the libration points or the Lagrange points exist in the CR3BP, denoted as L_i for $i = 1, ..., 5$. Although a closed-form solution does not exist for the equations of motion in the CR3BP, one integral of the motion aids numerical analyses. This quantity is termed the Jacobi constant and is evaluated as a function of the pseudo-potential and the velocity magnitude for P_3 in the rotating frame, v, as $C = 2U^* - v^2$. Bounds on the allowable motion of P_3 at a given Jacobi constant value are indicated via three-dimensional Zero Velocity Surfaces (ZVSs) and planar Zero Velocity Curves (ZVCs) in configuration space. Regions that are inaccessible at given energies are termed the *forbidden regions*, and a change in velocity (energy) is necessary to access these regions.

N-Body Ephemeris Model

The N-body ephemeris model offers a higher level of fidelity than the CR3BP, allowing the addition of other celestial bodies that influence the motion of a spacecraft. Contrary to the formulation of the CR3BP, the ephemeris model is based in an inertial frame, centered on some central body denoted P_q. The spacecraft, denoted P_i, is assumed to move under the gravitational effect of this central body, as well as other influential celestial bodies, denoted P_j. As in the CR3BP, all bodies are modeled as point masses. The true locations of the bodies that comprise the N-body model,

both relative to the spacecraft and to the central body, yield a more accurate representation of the dynamical motion of the spacecraft. The relevant equations of motion that govern the spacecraft dynamics are second order vector differential equations, i.e.,

$$\ddot{\bar{r}}_{qi} = -G\frac{(m_i + m_q)}{r_{qi}^3}\bar{r}_{qi} + G\sum_{\substack{j=1 \\ j\neq i,q}}^{N} m_j \left(\frac{\bar{r}_{ij}}{r_{ij}^3} - \frac{\bar{r}_{qj}}{r_{qj}^3}\right) \tag{3}$$

where $\bar{r}_{qi}$ represents the position of the spacecraft relative to the central body, $\bar{r}_{ij}$ denotes the position of each perturbing body with respect to the spacecraft, and $\bar{r}_{qj}$ denotes the position of each perturbing body relative to the central body. The DE421 planetary ephemerides retrieved from the NASA Jet Propulsion Lab (JPL) Navigation and Ancillary Information Facility (NAIF) are utilized to obtain the relative positions and velocities of the various celestial bodies in this model.[7] In the context of modeling spacecraft motion in the cislunar dynamical environment, it is generally reasonable to select the Earth as the central body, with additional perturbing effects resulting from the inclusion of the Moon, the Sun, and Jupiter.

EARTH-MOON RESONANT ORBITS

Resonant orbits are favorable for surveillance-based applications, especially due to the broad areas potentially swept by the unique geometries of such orbits. The orbits are characterized by their resonance ratio, denoted p:q. Within the context of the Earth-Moon dynamical system, a spacecraft in a p:q resonant orbit completes approximately p revolutions of the Earth in the time that the Moon orbits the Earth q times. A wide variety of resonant orbits are identified for their potential applications spanning cislunar space.[6,8] Resonant orbits classified by a p:q ratio such that $p > q$ are termed interior resonant orbits, and spacecraft in these orbits remain interior to the Earth-Moon system. For ratios where $p < q$, the orbits are termed exterior resonances, and spacecraft in such orbits are characterized by longer periods and geometries that span the exterior of the Earth-Moon system.

Retrograde Resonant Orbits

One family of retrograde resonant orbits, identified in Figure 2, is computed in the Earth-Moon CR3BP dynamical model and corresponds to a 2:1 resonance ratio. The period of each orbit in the Earth-Moon rotating frame as illustrated in Figure 2(a) is approximately equal to the lunar sidereal period of $27.3\ days$. In the Earth-centered inertial frame view in Figure 2(b), each *elliptical lobe*, thus, corresponds to roughly half the lunar sidereal period. The inertial frame emphasizes the retrograde nature of these orbits relative to the Earth. Each orbit is colored by its Jacobi constant value; due to the retrograde nature of this orbit family, these orbits are characterized by low Jacobi constant values and, thus, possess relatively higher energies. In the inertial frame view, it is noted that orbits possessing higher values of Jacobi constant visibly precess after their lunar encounters. This characteristic, predictably, only appears for orbits with smaller perigee and perilune radii that appear to be more "eccentric" in the inertial frame. Additionally, orbits in this family possessing higher Jacobi constant values tend to be unstable in the linear sense. Nonetheless, their associated stability indices are not sufficiently high to reflect the existence of strong stable and unstable manifolds.[6] Because of their characteristic low Jacobi constant (high energy) values, transfers to and from other dynamical structures and orbits of interest necessitate significant propellant costs.[6] However, these properties render these 2:1 orbits operationally stable and potentially useful for surveillance missions. The

2:1 retrograde resonant orbits are one example of resonant orbits that transit the GEO-Moon region. While the scope of analysis in this investigation is limited to the 2:1 resonances, other resonant orbits exist that present cislunar surveillance opportunities as well.

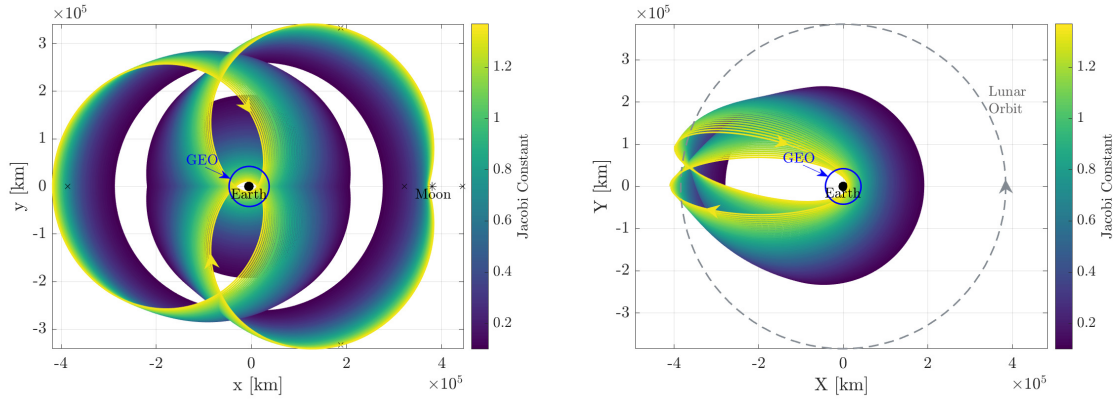

(a) Earth-Moon rotating frame.

(b) Earth-centered inertial frame.

Figure 2. Family of 2:1 retrograde resonant orbits computed in the Earth-Moon CR3BP and colored by their Jacobi constant values.

As evident in Figure 2, orbits in this family pass close to the Earth, and specifically, one orbit possesses a perigee radius equal to the radius of a geosynchronous orbit (GEO) in the retrograde direction. In addition to providing access to GEO, the same orbit spans out to the vicinity of the Moon and the L_1 libration point on the Earth-outbound leg. Since the orbit is periodic, this GEO-Moon passage recurs with every revolution, approximately once every lunar sidereal period. As such, a surveillance satellite in this orbit, under natural dynamical motion, provides repeated direct links between the more familiar GEO region, and the outer reaches of cislunar space in the neighborhood of the lunar orbit. Due to this favorable motion connecting these high-interest cislunar subspaces, this particular orbit, with a perigee radius approximately equal to $42,164\ km$, is selected as the *chief* orbit for further analysis. The orbit possesses a period of $25.96\ days$ and a Jacobi constant value of 0.8964. While its period is not precisely equal to the lunar sidereal period, the orbit is closed and periodic as observed in the rotating frame. The time-of-flight between the GEO belt and the perilune radius of the orbit, and vice versa, is approximately $7.15\ days$. A spacecraft in this orbit is able to depart the Earth from the GEO region in the retrograde direction, approach the Moon to within $8,500\ km$ of the lunar surface, and return to the GEO belt, again in the retrograde direction, within a $14.3\ day$ time frame. Again, it is noted that due to the periodicity of the orbit, this $14.3\ day$ span of a GEO-Moon-GEO transit repeats approximately once a month as well. Another long-term advantage of the orbit is that due to the lunar sidereal resonance, the precession seen in the inertial frame persists with subsequent revolutions as well. When the chief orbit is propagated for about 20 revolutions (approximately $507\ days$) using the CR3BP equations of motion, the orbit completely maps out the Earth-Moon planar subspace of the cislunar region without deviations from its inherent geometry.

For the purposes of surveying cislunar space, it is also useful to consider multiple spacecraft that, together, support a network of space-based sensors. Such a constellation is particularly necessary for cislunar SDA, owing to the vastness of this region. Orbits in 2:1 retrograde resonance with the

Moon, for instance the chief orbit identified above, offer one option for the "hub" of a network of sensors. The natural sidereal resonance allows the accessibility between the geostationary region and the lunar vicinity to persist for multiple revolutions. An additional advantage of the orbit, arising due to this resonance, is that the relative configuration with other spacecraft in similar orbits is sustained with subsequent revolutions as well. Thus, additional surveillance spacecraft harboring space-based sensors in orbits from this family naturally remain in the relative vicinity of the chief spacecraft.

As an illustrative example, a second orbit from this 2:1 retrograde resonant family is selected, termed the *deputy* orbit. The Jacobi constant value of this orbit is approximately 0.8721, and its period is $25.96\ days$. Recall that both orbits are ballistic; no maneuvers are included in this CR3BP trajectory. It is noted that while the selection of a deputy orbit is free, the orbit in this investigation is determined such that the spacecraft remains within reasonable proximity of the chief orbit. To demonstrate a long-term surveillance scenario, both orbits are propagated for 20 revolutions. Figure 3(a) illustrates the chief orbit in black, along with the deputy orbit in red, as they appear in the Earth-Moon rotating frame. Figure 3(b) illustrates an Earth-centered inertial frame view, where the multiple revolutions of the orbits are more apparent. The natural 2:1 sidereal resonance causes the orbits to continually precess in the retrograde direction, eventually repeating onto themselves in the inertial frame as well. Figure 4 represents the spacecraft separation and the distance to the Moon over the full 507 day period. The isochronous distance between the chief and the deputy, as plotted in Figure 4(a), remains bounded between $350\ km$ and $8,500\ km$, with their closest relative distance occurring at perilune. Similarly, due to their resonance with the lunar orbit, the spacecraft maintain similar distances with respect to the Moon over the course of the 20-revolution period. The closest approach with the Moon occurs at an altitude of approximately $8,400\ km$ for the chief orbit, and at $8,700\ km$ for the deputy. Notably, the link between the vicinity of the Earth near GEO and the lunar vicinity is preserved for both the orbits over 20 revolutions, yielding opportunities for GEO-Moon-GEO transit once every month.

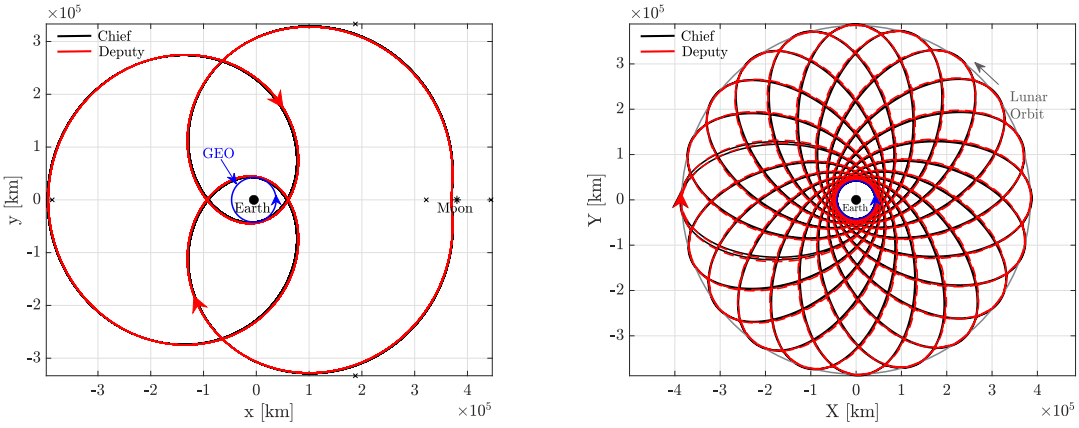

(a) Earth-Moon rotating frame.

(b) Earth-centered inertial frame.

Figure 3. Chief (black) and deputy (red) orbits as seen in the rotating and inertial frames. Both orbits are propagated for 20 revolutions. Model: Earth-Moon CR3BP.

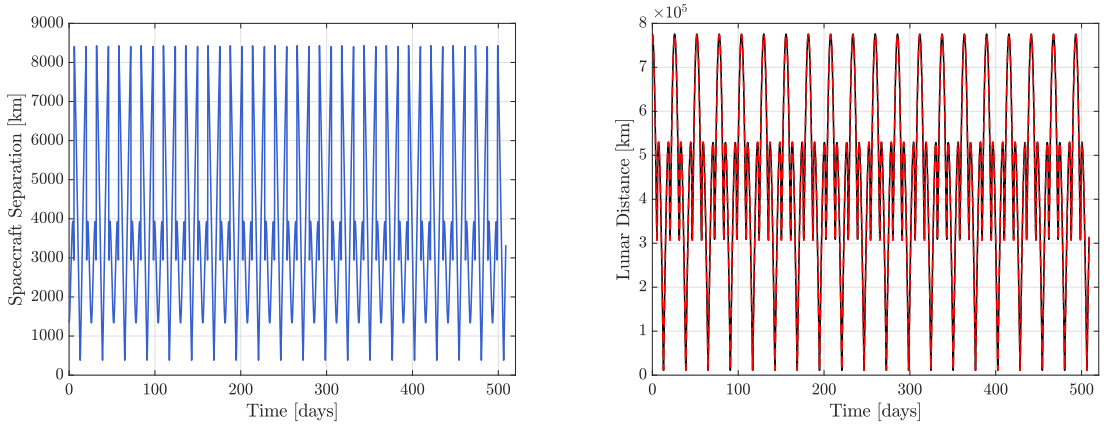

(a) Spacecraft separation.

(b) Lunar distance.

Figure 4. Spacecraft separation and lunar distance for 20 revolutions or 507 days in the CR3BP.

Ephemeris Validation for Sustained Cislunar Operations

Additional insight is gained by analyzing the chief and the deputy orbits in the N-body ephemeris model. However, the accuracy and fidelity of the ephemeris model demands careful consideration of the desired characteristics. In this investigation, to maintain the resonance of the selected orbits and, by extension, to maintain the relative configuration of the chief-deputy constellation, the goal of the ephemeris transition process is the preservation of the baseline geometry from the CR3BP trajectory over multiple revolutions in the N-body model. The transition approach employed in this investigation involves a stacking process, in which multiple revolutions of the CR3BP orbit are stacked and discretized.[9] Continuity in position and velocity (barring any allowed intermediate maneuvers) is enforced in the ephemeris model via a differential corrections scheme. Periodic orbits from the CR3BP transition into quasi-periodic trajectories in the ephemeris model, ideally reflecting the inherent CR3BP geometry.

In this investigation, the long-term behavior of spacecraft in the chief and deputy orbits is modeled via an Earth-Moon-Sun-Jupiter ephemeris model, with the Earth being the central body. To select the model epoch, the instantaneous distance between the Earth and the Moon, that is equal to the CR3BP characteristic length, l^*, is plotted over the course of one year. The epoch associated with the smallest deviation from the CR3BP l^*, indicated by the horizontal line in Figure 5, is selected as the epoch for the ephemeris model. For the value of l^* in this investigation, and considering dates in the year 2025, the appropriate epoch is located as February 24, 2025, 00:00:00 UTC, indicated by the green circle in Figure 5. Since the process of constructing the ephemeris trajectory relies on the CR3BP solution, this epoch aids the targeting process. For an application that requires a different epoch, the previous ephemeris trajectory produced at a nearby epoch corresponding to the value of l^* is supplied as the initial guess for a subsequent targeting and/or continuation process.

To replicate the full mapping of the inertial frame seen in Figure 3(b), the same CR3BP stack of 20 revolutions of the chief and deputy orbits is seeded into the ephemeris multiple shooting scheme. Considering the duration of the full 20-revolution stack, about 507 $days$ for each trajectory, the multiple shooting algorithm incorporates intermediate maneuvers along the trajectory to aid the convergence process. In this case, four maneuvers of 100 m/s each are initially allowed over the

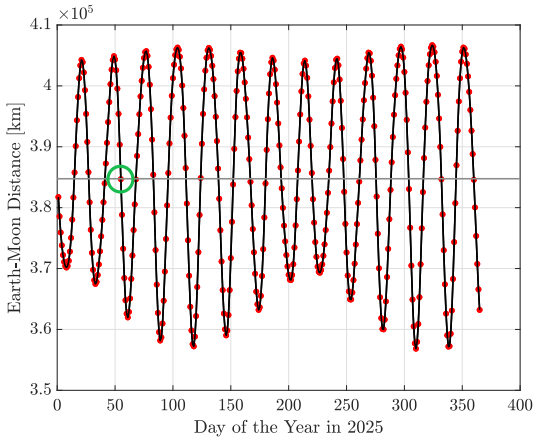

Figure 5. Selection of the epoch for the ephemeris model.

course of the full stack. The resulting converged ephemeris trajectory is then supplied as an initial guess to target the same trajectory with a reduced allowable maneuver limit. Incrementally stepping down the maneuver limit, a completely ballistic ephemeris trajectory that is analogous to the ballistic CR3BP 20-revolution stack is produced for both orbits.

The resulting ephemeris trajectories for both the chief and the deputy spacecraft appear in Figure 6. The Earth-Moon rotating frame view is plotted in Figure 6(a), and the J2000 Earth-centered inertial view of the trajectories appears in Figure 6(b). Note that while only the $\hat{x}$-$\hat{y}$ and $\hat{X}$-$\hat{Y}$ projections of the trajectories are plotted here, the trajectories are spatial in both frames. It is also apparent from both views in Figure 6 that the ephemeris trajectories for both spacecraft remain fairly bonded to their inherent CR3BP geometries, aided by the stacking corrections process. Additionally, recall that in the CR3BP, the 20-revolution trajectory maps the entirety of cislunar space (in the Earth-Moon plane) in approximately $507\ days$; in this ephemeris model, the same pattern appears over the course of $523\ days$. The ephemeris validation reveals additional possible advantages of these retrograde resonances for space-based sensor applications. The clear recurring passageway between the GEO region and the lunar vicinity persists without deterministic maneuvers along the baseline paths. Observe that the chief and deputy perigee radii remain tangent to, or in the proximity of, the geosynchronous orbit radius.

It is also useful to compare the distance between the chief and deputy spacecraft in the ephemeris model over the course of the 20-revolution period. Figure 7(a) illustrates the distance between the spacecraft, while Figure 7(b) depicts the evolution of the relative lunar distance over time. The bounds on the spacecraft distance are generally consistent with the values observed in the CR3BP. There are notable spikes in the relative distance between the two spacecraft, and these increased distances occur at perigee. These increases reflect a phase difference as the trajectories remain close. The strategies detailed by Davis et al. can be implemented to target periapsis times and mitigate the increased phase difference.[10] For the distance relative to the Moon over time, the amplitudes of variation are approximately the same as those seen in the CR3BP. In Figure 7(b), two amplitudes arise over time along the trajectory: when the spacecraft i) cross the Earth-Moon syzygy axis, and ii) approach perigee along the GEO region. In the CR3BP, the closest approach to the Moon occurs at the altitudes of $8,400\ km$ and $8,700\ km$ for the chief and the deputy, respectively; the same values drop to about $7,581\ km$ and $8,289\ km$ for the two spacecraft in the ephemeris model.

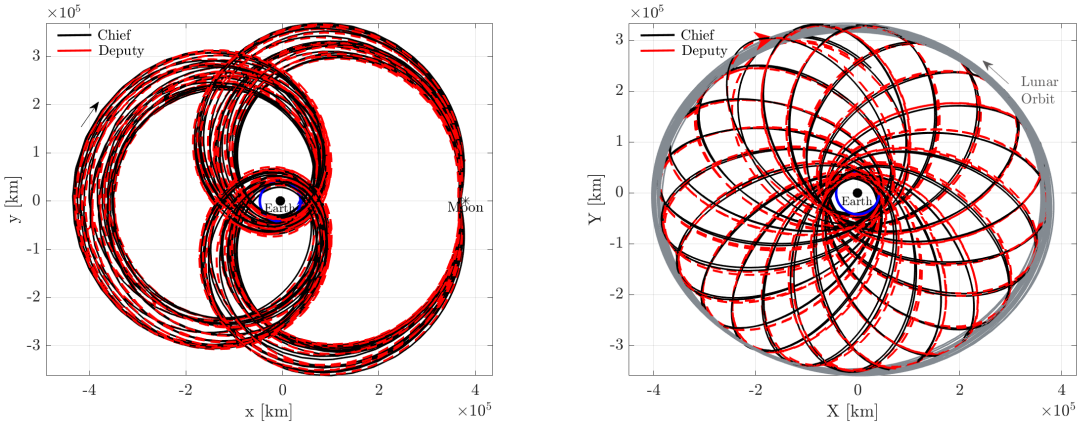

(a) Earth-Moon rotating frame.

(b) Earth-centered inertial frame.

Figure 6. Ephemeris analogs for chief (black) and deputy (red) orbits as viewed in the Earth-Moon rotating and the Earth-centered inertial J2000 frames. The lunar orbit in the inertial frame appears in grey. Model: Earth-Moon-Sun-Jupiter ephemeris. Model epoch: February 24, 2025, 00:00:00.

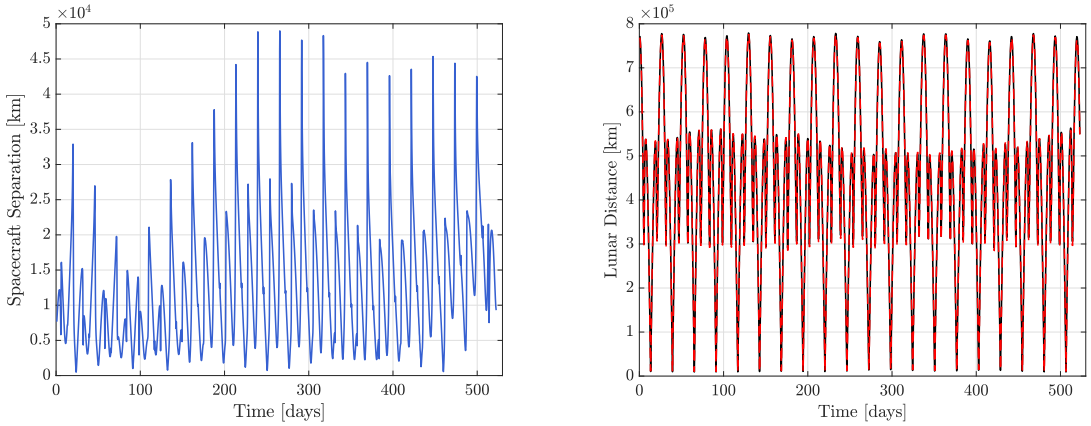

(a) Spacecraft separation.

(b) Lunar distance.

Figure 7. Spacecraft separation and relative lunar distances for 20 revolutions or 523 days. Model: Earth-Moon-Sun-Jupiter ephemeris. Model epoch: February 24, 2025, 00:00:00.

Prograde Resonant Orbits

The chief and deputy orbits and, in general, other orbits from the retrograde family of 2:1 resonances, do not circumvent the lunar orbit. As such, access to the near-side of the Moon only is directly available via these orbits. However, other options for resonant orbits are available that, while not circumlunar themselves, possess stable and unstable manifolds that allow access to the far side of the Moon. For instance, there exist orbits in a similar family of 2:1 sidereal resonances that orbit the Earth in the prograde direction. These orbits are linearly unstable and, thus, offer options to transfer in and out of other dynamical structures in the lunar vicinity.

The family of prograde 2:1 resonant orbits, computed in the Earth-Moon CR3BP, is plotted in

Figure 8, with the orbits colored by their respective Jacobi constant values. Naturally, these orbits complete two revolutions of the Earth during one sidereal period of the Moon. However, as evident in Figure 8(b), their motion relative to the Earth proceeds in the prograde direction. In Figure 8(a), the orbit family is viewed in the Earth-Moon rotating frame, with options supporting the high-interest passageway from the geosynchronous belt to the lunar vicinity and return. The range of Jacobi constant values spanned by orbits in this family is higher than its retrograde counterpart. However, in general, these orbits tend to be linearly unstable and, thus, lead to stable and unstable manifolds that further extend the natural reaches of spacecraft moving along these orbits.

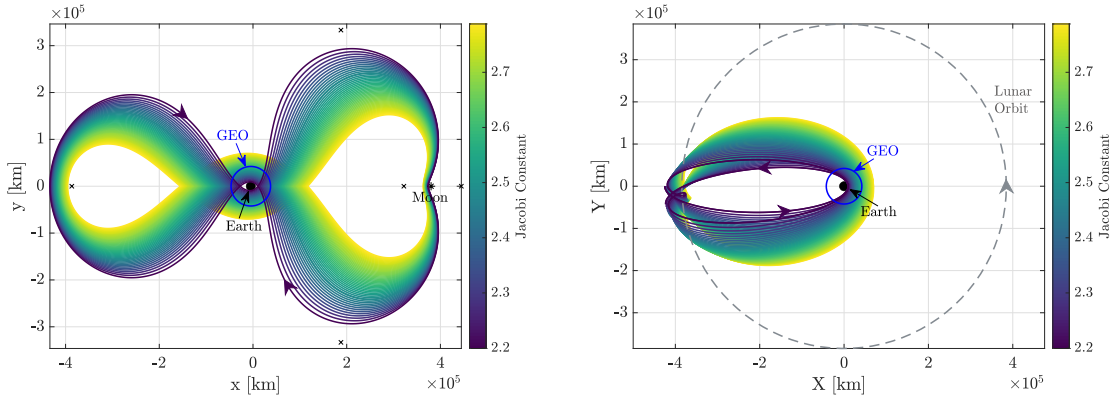

(a) Earth-Moon rotating frame.

(b) Earth-centered inertial frame.

Figure 8. Family of 2:1 prograde resonant orbits in the Earth-Moon system.

Similar to the retrograde resonant orbit family, there exists a member orbit in this prograde family as well that possesses a perigee radius equal to the geosynchronous orbit radius. This particular orbit is described with a Jacobi constant value of 2.5946, and a period approximately equal to the lunar sidereal period, $28.13\ days$. Additionally, this particular orbit is linearly unstable. The extent of instability of the orbit is evaluated using the stability index, defined in this investigation as,

$$\nu_i = \frac{1}{2}\left(\lambda_i + \frac{1}{\lambda_i}\right) \tag{4}$$

where λ_i denotes one of the six eigenvalues of the monodromy matrix for the periodic orbit.[11] Note that in the CR3BP dynamical model, the eigenvalues of the monodromy matrix occur in reciprocal pairs. As such, three unique stability indices characterize an orbit, at least one of which equals unity due to orbital periodicity. For the selected orbit from the prograde 2:1 resonant family, the value for the maximum stability index is 48.13, indicative of the existence of manifolds that flow in and out of the orbit. This natural flow is leveraged to locate transfer trajectories originating from the 2:1 resonance that also offer periodic circumlunar access. Homoclinic-type periodic orbit chains are constructed that extend the range of access to the lunar far side. This characteristic may be favorable for various commercial and government purposes, considering the challenges posed by the lack of Earth-communication in the region.

Homoclinic-Type Periodic Orbits

Noting the instability of the selected prograde resonant orbit, its invariant manifolds are constructed to identify excursions in and out of the orbit. Trajectories that lie on its stable manifold asymptotically approach the orbit over time, while trajectories on its unstable manifold depart the orbit when propagated in forward time. However, the process of analyzing trajectories on invariant manifolds in configuration space is challenging due to their tangled and complex geometries. Thus, Poincaré maps are employed to locate useful trajectories on the manifolds. In this investigation, Poincaré maps are constructed by locating the hyperplane, Σ, at $y = 0$. The Jacobi constant value for the map is fixed and, in this case, is equal to the Jacobi constant of the selected 2:1 resonance at $C = 2.5946$. The intersections with the hyperplane of the trajectories on the stable and unstable manifolds are recorded. Since the orbit and its manifold trajectories are planar, the full 4-dimensional state corresponding to each intersection with the hyperplane is available.

The x-$\dot{x}$ projection of the Poincaré map appears in Figure 9(a). It is associated with trajectories asymptotic to the stable (teal) and unstable (magenta) manifolds for the selected 2:1 resonant orbit. Of particular interest are the locations where the stable and unstable returns intersect on the map, as they indicate the existence of a homoclinic connection to the orbit. A homoclinic connection is a maneuver-free transfer trajectory that connects the orbit to itself, allowing deviations from the orbit geometry while guaranteeing a return to the periodic orbit. While the Poincaré map depicts several such connections, the intersection highlighted by the white box in Figure 9(a) is a focus for further analysis. Since it corresponds to an $\hat{x}$-value beyond the Moon, the underlying trajectories are *circumlunar*, that is desirable for excursions from the original *cislunar* 2:1 resonant orbit. The intersection of returns from the map is then propagated forwards and backwards in time to yield a homoclinic connection to the 2:1 resonant orbit, as illustrated in Figure 9(b). The teal trajectory is asymptotic to the stable manifold, and the magenta trajectory is asymptotic to the unstable manifold. The underlying 2:1 orbit appears in black as well. Clearly, the homoclinic connection preserves the geometry of the orbit, but with an acceptable deviation that allows circumlunar transit. Notably as well, the deviation in the original orbit geometry originates from a Moon-centered orbit, that is identified as belonging to the family H_1 (also family *g*).[12,13] Considering that the homoclinic connection occurs at a perpendicular crossing of the $\hat{x}$-axis, it is then possible to apply differential corrections to produce an orbit that shadows the magenta and teal trajectories. The resulting periodic orbit, thus, reflects the dynamics of both the 2:1 resonant orbit and the orbit from the H_1 family. This overlap in the manifold structure of the prograde 2:1 orbit with the H_1 orbit hints at a similarity in their respective manifolds at this energy level.

The corrected periodic orbit resulting from the homoclinic connection appears in Figure 10(a). This homoclinic-type orbit possesses a period of approximately $87.93\ days$, a significant increase from the lunar sidereal period. At $C = 2.5394$, this particular orbit chain possesses a higher Jacobi constant value than the retrograde resonant chief orbit and, thus, possesses lower energy. However, as evident in Figure 10(a), the combined prograde 2:1-H_1 orbit remains tangent to the geosynchronous orbit radius at periapsis. Additionally, as is true for all periodic orbits computed in the CR3BP, this homoclinic-type periodic orbit belongs to a family of other similar periodic orbits. Figure 10(b) illustrates a subset of the orbit family as visualized in the Earth-Moon rotating frame, with the orbits colored by their respective Jacobi constant values. Evidently, the $\hat{y}$-amplitude of the orbits reduces significantly as the Jacobi constant increases, indicating a decrease in the orbit period as well. The perigee radius increases, while the perilune radius decreases with an increase in Jacobi constant, with the smallest orbits shrinking closer to the lunar vicinity. It is noted that the

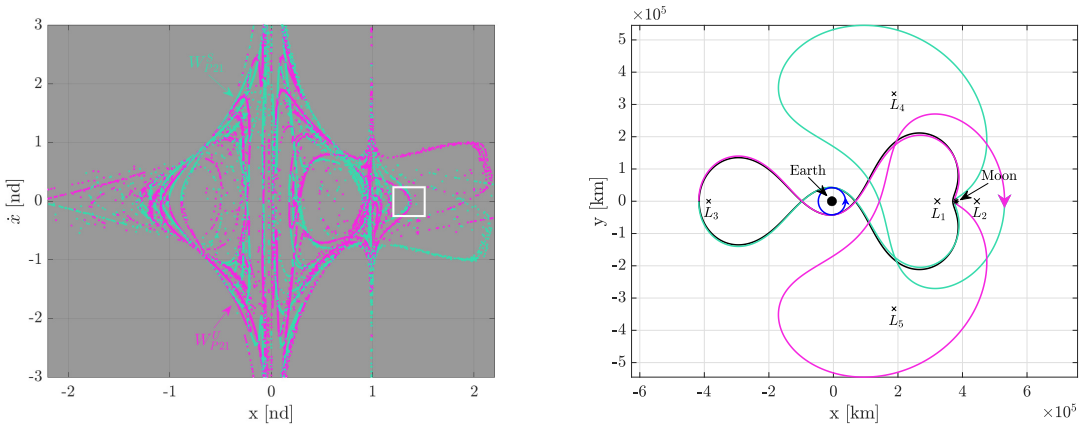

(a) Poincaré map. (b) Earth-Moon rotating frame.

Figure 9. Poincaré section for trajectories on the stable (teal) and unstable (magenta) manifold of the selected prograde 2:1 resonant orbit. The highlighted intersection of manifold returns is propagated forwards and backwards in time to reveal a homoclinic connection to the orbit.

extent of the prograde 2:1-H_1 orbit family is restricted to the energy levels at which the underlying homoclinic connection exists. Figure 11 illustrates Poincaré maps for prograde 2:1 resonant orbits computed at various Jacobi constant values. In Figure 11(a), Figure 11(b), and Figure 11(c), the white box indicates the location of the 2:1-H_1 homoclinic connection at each energy level. With increasing values of Jacobi constant, the homoclinic connections move inward as well, which is expected considering the reducing perilune radii seen in Figure 10(b). At the Jacobi constant value of $C = 3.0946$, while there exist other homoclinic connections, the intersection that results in the 2:1-H_1 combined periodic orbit does not exist. Additionally, while the 2:1-H_1 chain is one example, other homoclinic-type periodic orbits exist that combine the prograde 2:1 resonance geometry with other periodic orbits.

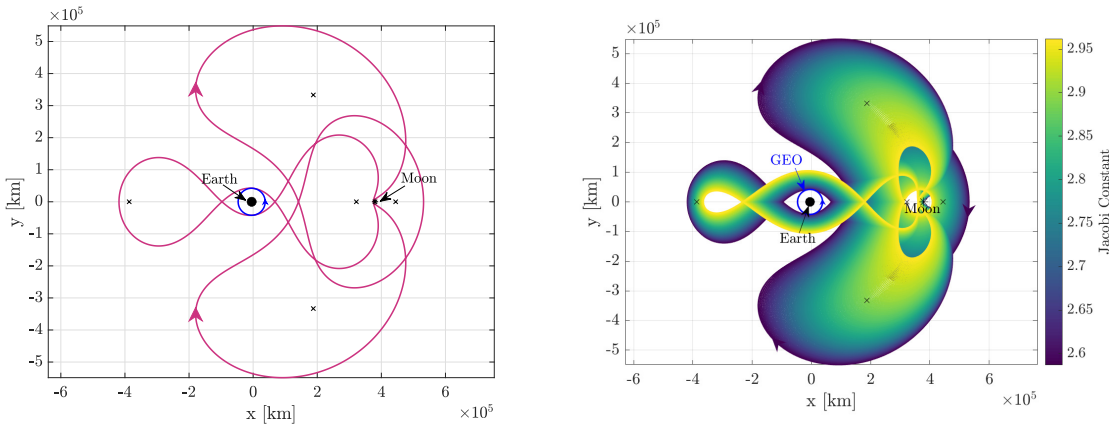

(a) Corrected periodic orbit. (b) Periodic orbit family.

Figure 10. A periodic orbit originating from a homoclinic connection to the prograde 2:1 resonant orbit. The new periodic orbit exhibits the geometry of orbits from the family H_1, and exists as a family of periodic orbits.

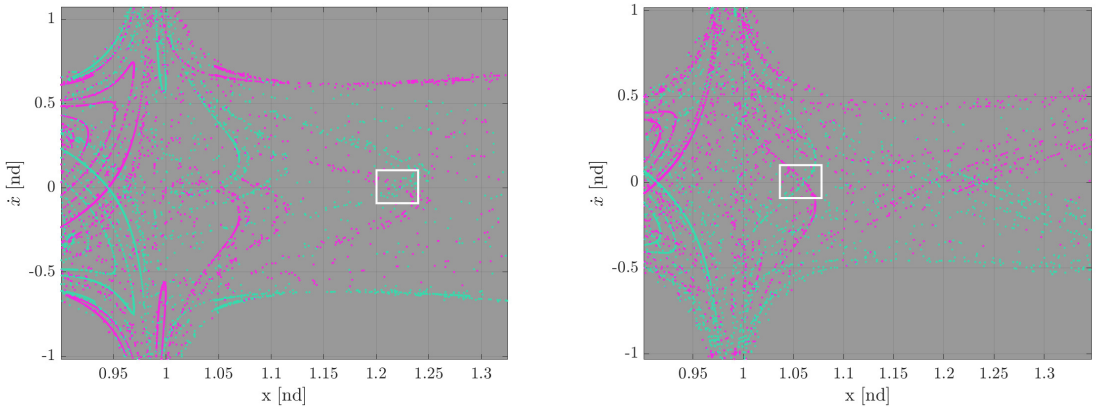

(a) $C = 2.7958$ (b) $C = 2.9615$

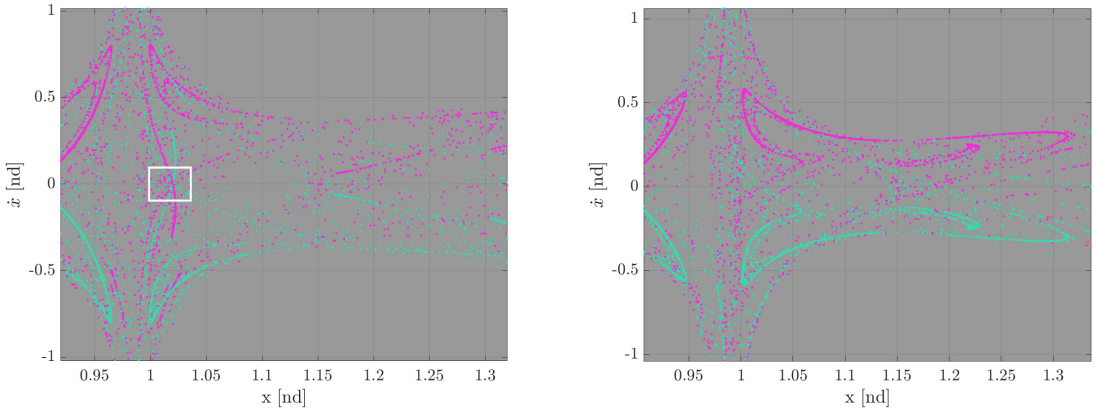

(c) $C = 3.0364$ (d) $C = 3.0946$

Figure 11. Poincaré maps for prograde 2:1 orbits at varying Jacobi constants. White boxes indicate the homoclinic connections that shadow H_1 orbits. This homoclinic connection does not exist at $C = 3.0946$.

Transfers between Prograde and Retrograde Resonant Orbits

In this investigation, two orbits in a 2:1 sidereal resonance with the Moon are identified, one retrograde relative to the Earth, and the other moving in the prograde direction. Both the selected orbits, however, possess perigee altitudes that are tangent to the geosynchronous radius. While the retrograde orbit provides near-stable characteristics, it does not offer line-of-sight to the lunar far side. Alternatively, the prograde resonant orbit yields circumlunar access via homoclinic connections due to its inherent instability. It is possible, then, to combine the individual capabilities of these orbits and compute options for transferring between them. For reference, Table 1 summarizes the characteristics of the selected prograde and retrograde resonant orbits.

Transfer scenarios between the two orbits in Table 1 appear in Figure 12. In each case, the retrograde 2:1 resonant orbit is plotted in grey, the prograde orbit appears in pink, and the transfer itinerary linking the two orbits is green. In Table 1, the difference in the Jacobi constant values for each orbit predicts a nontrivial maneuver to connect them. The maneuver location for each case is indicated by the solid green marker. The direct transfer departing the retrograde orbit and arriving

Table 1. Characteristics of the selected resonant orbits.

Orbit	Jacobi Constant	Period [days]	Stability Index
Retrograde 2:1 (Chief)	0.8964	25.96	8.59
Prograde 2:1	2.5946	28.13	48.13

at its prograde counterpart appears in Figure 12(a), with a maneuver at perilune of $608.03\ m/s$. The reverse scenario, i.e., from the prograde resonance to the retrograde orbit, appears in Figure 12(b). This case necessitates a maneuver of $612.48\ m/s$. The tangency with GEO and the perilune radius is preserved for both. The availability of direct transfers between these two orbits expands their potential for applications. It is also possible to depart the geosynchronous radius in the retrograde direction and, with a ΔV at perilune, return to the same perigee, but in the prograde direction. Naturally, the opposite path is also demonstrated. Additional viable applications include transferring from the retrograde orbit to the prograde orbit, and eventually allowing circumlunar excursions via the prograde 2:1-H_1 orbit chain.

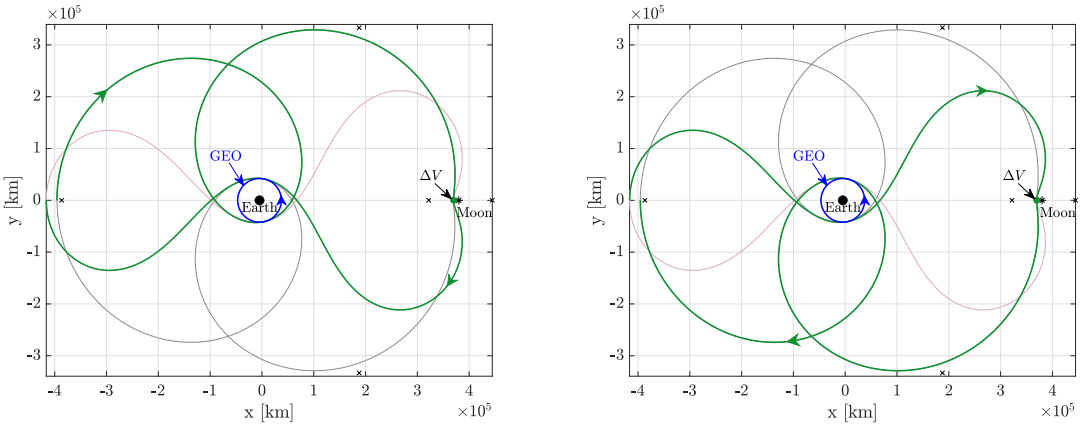

(a) Retrograde to prograde.

(b) Prograde to retrograde.

Figure 12. Transfers between the retrograde and prograde 2:1 resonant orbits as seen in the Earth-Moon rotating frame.

LUNAR FREE RETURNS

Options for transfers from the vicinity of the Earth to the Moon also include lunar free returns. Noting their relationship with resonant orbits,[14] it is especially useful to assess their transfer times and energy levels against the 2:1 resonant orbits investigated here. Within the context of cislunar space, lunar free returns are trajectories that transfer from the Earth to the lunar vicinity and, without requiring any propulsive maneuvers, return to the Earth vicinity.[15] These trajectories were exploited in the Apollo era, guaranteeing crew return in case of emergencies or communications disruptions. For surveillance-based missions, such trajectories are also potential avenues for transfer options between the Earth and the Moon, without risking the loss of the spacecraft. Thus, lunar free returns are typically constructed from an Earth-centered departure ellipse and a Moon-centered hyperbola, where the hyperbola shifts the velocity vector by a sufficient amount to guarantee an Earth return. Because of the close proximity to both the Earth and the Moon, the CR3BP serves as the appropriate

dynamical model in the generation of such trajectories. Lunar free returns are characterized as being either cislunar, where the perilune lies between the Earth and the Moon, or circumlunar, with a perilune that occurs on the lunar far side. These trajectories also exhibit varying characteristics depending upon whether their Earth-departure orbits are prograde or retrograde. Finally, while spatial free returns exist, only Earth-Moon planar trajectories are investigated here.[9]

Free returns in the CR3BP were originally analyzed in-depth by Schwaniger in 1963,[14] who numerically targeted free returns in the Earth-Moon system. More recently, Jesick and Ocampo detail an automated methodology for the generation of free returns, employing initial guesses from Keplerian analysis.[15] In this investigation, the methodology implemented by Pavlak is adopted in the generation of planar free return trajectories in the Earth-Moon CR3BP.[9] This approach relies on transitioning a two-body initial guess to the CR3BP using differential corrections. The process initiates at the periapsis of the Earth-centered ellipse, termed the translunar injection (TLI) point. A quick summary of the process is as follows:

1. The initial Earth-centered TLI states are determined in the inertial frame.
2. The states are transformed to the Earth-Moon rotating frame, centered on their barycenter.
3. The trajectory is propagated to produce the final velocity at a crossing of the $\hat{x}$-axis near the Moon.
4. Differential corrections are applied to render the $\hat{x}$-component of the final velocity equal to zero, yielding a perpendicular crossing of the $\hat{x}$-axis.

Since these free returns are symmetric, only the outbound leg of the trajectory is targeted numerically. The steps above, however, do not allow the freedom of selecting perigee/perilune altitudes outright. Thus, additional constraints, namely Earth departure altitude, lunar arrival altitude, and Earth departure flight path angle are incorporated into the multiple shooting scheme.[9] Once a lunar free return trajectory is generated, natural parameter continuation in the perigee/perilune altitude produces *families* of free returns. For instance, consider an Earth-departure altitude of $176.5\ km$ and a fixed Earth-departure flight path angle of 0°. Then, perilune altitudes are varied to construct a family of free return trajectories. These families are either cislunar or circumlunar, and depart from prograde Earth orbits or retrograde Earth orbits. All four cases appear, plotted in the Earth-Moon rotating frame, in Figure 13. For clarity in their geometries, only the Earth-outbound legs of all free returns appear. Additionally, while there exists a perpendicular crossing of the $\hat{x}$-axis at perilune for all trajectories, the departure from Earth is *not* a perpendicular crossing. Thus, at the TLI point and at the end of the symmetric Earth-inbound leg (not shown), the trajectories do not close, i.e., they are not periodic orbits. In each family in Figure 13, the lunar arrival altitude varies between $1,000\ km$ and up to $20,000\ km$. Each trajectory is colored by its Jacobi constant value.

The variation in the one-way time-of-flight and the associated Jacobi constant value for each of the four free return cases is plotted in Figure 14 as a function of the perilune radius. In each plot, the solid curves represent prograde departures from the Earth departure orbit, while retrograde departures are reflected along the dashed curves. Figure 14(a) represents the characteristics of circumlunar free returns, where the one-way time-of-flight (TOF) increases as the perilune radius increases as well. There is a significant Jacobi constant gap in the prograde-departure (solid) and retrograde-departure (dashed) curves, due to the high energy of the retrograde trajectories. These

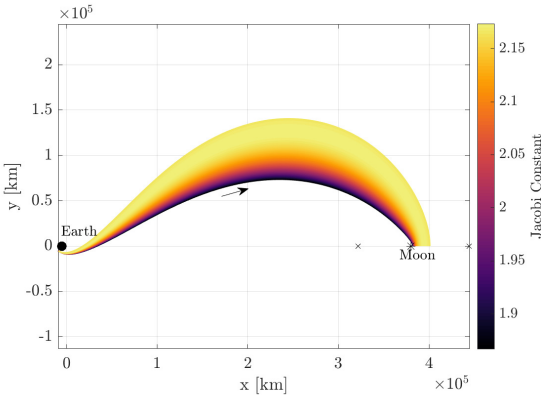

(a) Circumlunar with prograde departure.

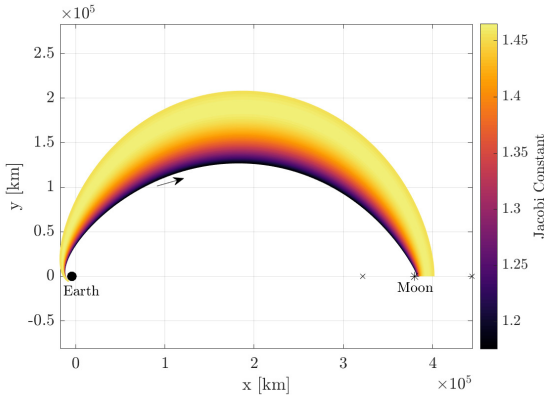

(b) Circumlunar with retrograde departure.

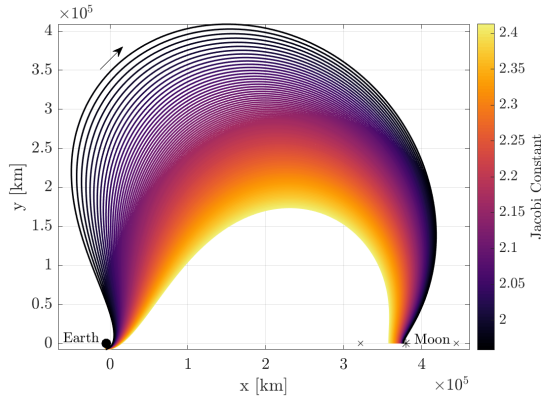

(c) Cislunar with prograde departure.

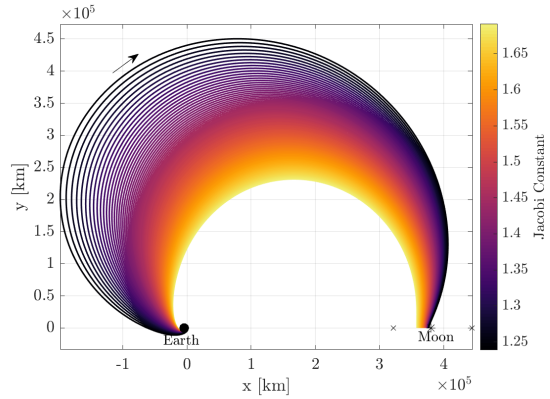

(d) Cislunar with retrograde departure.

Figure 13. Families of lunar free return trajectories departing from a 176.5 km altitude Earth orbit. Model: Earth-Moon CR3BP.

planar free returns that depart the Earth along the prograde direction arrive at their respective lunar orbits faster than the trajectories departing the Earth in the retrograde direction. In general, the circumlunar free returns exhibit relative short times-of-flight, bounded between 3 and 4.7 $days$. Similarly, Figure 14(b) summarizes the characteristics of the cislunar free returns plotted in Figure 13. It is immediately apparent that for departures from the same Earth orbit, cislunar free returns require a significantly longer TOF to arrive at the lunar orbit than their circumlunar counterparts. The TOF ranges spanned by these trajectories lies between 5 and 14 $days$. Additionally, the times-of-flight are reduced as a function of increasing perilune radius, also evident in Figure 13(c) and Figure 13(d), where the $\hat{y}$-amplitude of the trajectories is reduced as the perilune moves further from the Moon. Finally, note that the plots in Figure 14 represent departures only from a 176.5 km Earth orbit; it is possible to generate other free return families with higher Earth-departure altitudes as well.

While circumlunar free returns provide lunar far side access, further analysis of the cislunar free returns yields comparisons against the 2:1 retrograde and prograde resonant orbits. Additional families of cislunar free returns demonstrate the differences in geometries as a result of variations in the Earth-departure altitude. These additional families are constructed from Earth-departure circu-

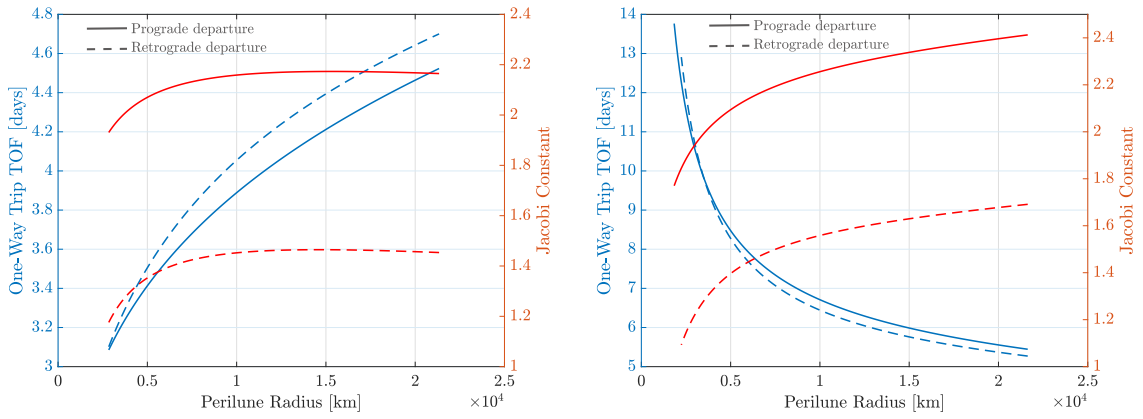

(a) Circumlunar free returns.

(b) Cislunar free returns.

Figure 14. Evolution of one-way time-of-flight and the Jacobi constant value for circumlunar and cislunar free returns as a function of the perilune radius. The Earth-departure orbit is fixed at an altitude of $176.5\ km$. The solid lines represent prograde departures, while dashed lines pertain to retrograde departures.

lar orbits of altitudes equal to $10,000\ km$, $20,000\ km$, $30,000\ km$, and $35,700\ km$. The latter corresponds to departure from the radius of a geosynchronous orbit. Selected lunar free returns from these additional families are plotted in Figure 15(a), where the blue trajectories correspond to prograde Earth departures, and the dark red trajectories depart retrograde relative to the Earth. It is immediately apparent that these trajectories, as viewed in configuration space, bear some resemblance to portions of the prograde and retrograde 2:1 resonant orbits computed previously. This resemblance is more obvious in Figure 15(b), where the prograde (blue) and retrograde (red) departures from a $10,000\ km$ Earth orbit appear. Also plotted are the 2:1 prograde (light blue) and retrograde (pink) orbits that possess a perigee altitude of $10,000\ km$. This similarity points to a relationship between certain lunar free returns and the 2:1 resonant orbits. Schwaniger mentions the existence of a free return trajectory that is actually a periodic orbit and approaches the Moon at a certain altitude once a month.[14] To be periodic, the free returns must cross the $\hat{x}$-axis perpendicularly at perilune; additionally, the Earth-outbound time-of-flight must be approximately one-fourth of the lunar sidereal period. In the trajectories in Figure 15(b), the times-of-flight are $7.97\ days$ and $7.37\ days$ for the prograde and retrograde departures, respectively. Thus, certain combinations of Earth-departure altitudes and lunar arrival altitudes for cislunar free returns yield periodic orbits that exist in a 2:1 sidereal resonance with the Moon. This fact is further confirmed by comparing the Jacobi constant values of the periodic lunar free returns with those of associated 2:1 resonant orbits, which are equal in both the prograde and retrograde cases.

Due to the constraints on the period of resonant orbits, not all lunar free returns are resonant periodic orbits. Specifically, it is demonstrated that circumlunar free returns are defined by shorter times-of-flight and, thus, cannot satisfy the natural resonance criterion. Cislunar free returns exhibit longer times-of-flight and, thus, lead to near-resonance orbital periods. Thus, the lunar free returns that are closed periodic orbits in the rotating frame exist in a 2:1 sidereal resonance with the Moon. These periodic free returns offer opportunities for inserting into lunar orbits once a month, however, only providing access to the near side of the Moon. Some periodic lunar free returns are overlaid with the families of prograde and retrograde 2:1 resonant orbits in Figure 16. The four free return

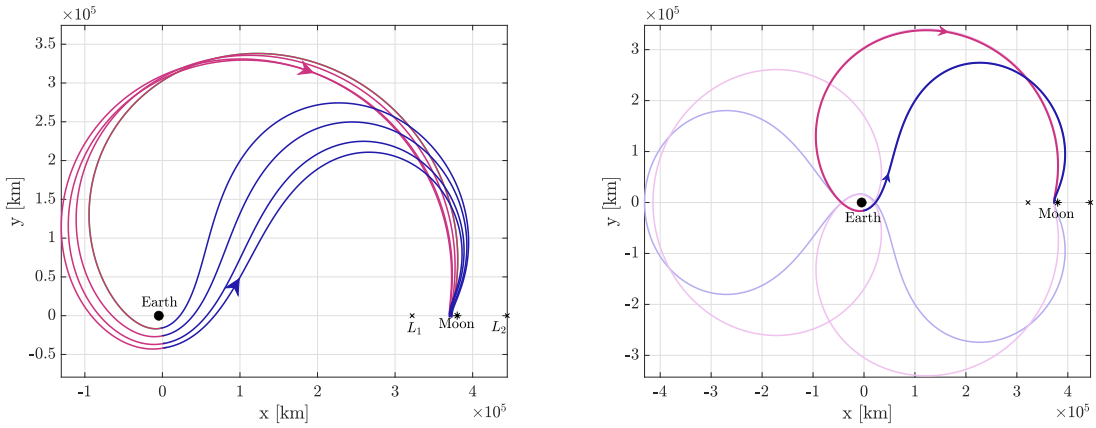

(a) Various departure altitudes.

(b) Similarity with resonant orbits.

Figure 15. Cislunar free returns departing from different Earth orbits. The blue trajectories represent prograde Earth departures and the dark red trajectories represent retrograde departures. The associated 2:1 resonant orbits appear in light blue (prograde) and pink (retrograde) on the right.

orbits depart the Earth from altitudes of $10,000\ km$, $20,000\ km$, $30,000\ km$, and $35,700\ km$. It is apparent, then, that the resonant orbits themselves are periodic lunar free returns. Progression along each orbit family corresponds to free returns with varying Earth departure and lunar arrival altitudes. Thus, such orbits supply recurring access between the Earth and the Moon, with options for both prograde and retrograde departures from the Earth.

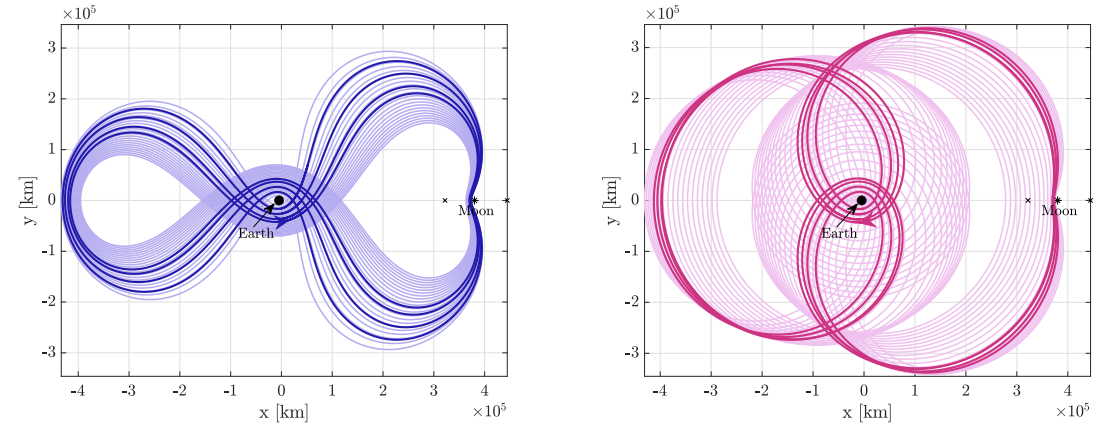

(a) Prograde similarity.

(b) Retrograde similarity.

Figure 16. Orbits from the prograde and retrograde 2:1 resonant families as seen in the Earth-Moon rotating frame appear in light blue and light pink. The darker colored orbits are periodic cislunar free returns departing from $10,000\ km$, $20,000\ km$, $30,000\ km$, and $35,700\ km$ altitude circular Earth orbits. Model: Earth-Moon CR3BP.

CONCLUDING REMARKS

Resonant orbits are demonstrated for their potential applicability for space domain awareness applications in cislunar space. Subsets of the families of both prograde and retrograde resonant orbits offer direct access between the geosynchronous orbit region and the vicinity of the Moon. The long-term behavior of the proposed orbits is analyzed within a higher-fidelity dynamical environment to assess their usefulness for mission design. It is noted that the retrograde 2:1 resonant orbit exhibits behavior that may be desirable for relative motion between two vehicles. A pair of chief and deputy spacecraft is demonstrated to simultaneously survey cislunar space via orbits from the retrograde resonance family. Their viability in the ephemeris model is evaluated, demonstrating that the orbital characteristics observed in the CR3BP dynamical model are preserved through the ephemeris transition process. In addition to surveilling cislunar space, spacecraft in such orbits expand the reach of cislunar excursions beyond the geosynchronous orbital region.

The linearly unstable prograde 2:1 resonant orbits offer direct line-of-sight access to the lunar far side. The manifolds corresponding to these orbits reveal connections with Moon-centered orbits that maintain local lunar access. By leveraging dynamical systems theory and Poincaré mapping techniques, various other periodic orbits are uncovered that extend trajectories past the lunar orbit as well. Transfers between the prograde and retrograde resonant orbits with similar perigee altitudes are demonstrated as an avenue for expanded mission applications.

Finally, lunar free return trajectories are computed in the Earth-Moon CR3BP as options for Earth-Moon "traffic lanes". Various departure options, for both Earth altitude and prograde or retrograde departure directions, are demonstrated for circumlunar and cislunar free returns. Cislunar free returns are similar to resonant orbits, and their relationship is further evaluated to reveal periodic lunar free returns in 2:1 sidereal resonance with the Moon. These transfer trajectories provide options of varying energies and times-of-flight for accessing the lunar vicinity from the Earth. While the options for transit times from the Earth to the vicinity of the Moon offered by circumlunar free returns are shortest, their coverage of cislunar space lacks compared to the options offered by resonant orbits. Even for cislunar free returns, while options might exist that allow for faster transit from the vicinity of the Earth to the Moon, those trajectories are neither periodic, nor provide cislunar coverage to the levels demonstrated by the resonant orbits.

ACKNOWLEDGEMENTS

The authors would like to thank the Purdue University School of Aeronautics and Astronautics for supporting this work. The authors also appreciate access to the computational facilities at the Barbara and Rune Eliasen Visualization Laboratory. Support is also appreciated under contract USAF FA8649-21-9-9004.

REFERENCES

[1] K. Johnson, "Fly Me to the Moon: Worldwide Cislunar and Lunar Missions," February, 2022. Center for Strategic and International Studies.

[2] D. Werner, "Updated intelligence report calls for improved monitoring of cislunar space," August, 2021. https://spacenews.com/dia-report-2021-cislunar-monitoring/, last accessed at 2022-03-26.

[3] J. Perkins, "AFRL's Cislunar Highway Patrol System seeks industry collaboration," March, 2022. https://www.505ccw.acc.af.mil/News/Article-Display/Article/2972971/afrls-cislunar-highway-patrol-system-seeks-industry-collaboration/, last accessed at 2022-03-26.

[4] C. Frueh, K. Howell, K. DeMars, and S. Bhadauria, "Cislunar Space Situational Awareness," *31st AIAA/AAS Space Flight Mechanics Meeting*, Charlotte, North Carolina (Virtual), February, 2021.

[5] C. Frueh, K. Howell, K. DeMars, S. Bhadauria, and M. Gupta, "Cislunar Space Traffic Management: Surveillance through Earth-Moon Resonance Orbits," *8th European Conference on Space Debris*, Virtual, April, 2021.

[6] M. Gupta, K. C. Howell, and C. Frueh, "Earth-Moon Multi-Body Orbits to Facilitate Cislunar Surveillance Activities," *AAS/AIAA Astrodynamics Specialist Conference*, Big Sky, Montana (Virtual), August, 2021.

[7] "The Navigation and Ancillary Information Facility – SPICE Data (SPICE Kernels)," July, 2022. https://naif.jpl.nasa.gov/naif/data.html, last accessed at 2022-07-15.

[8] M. Vaquero, *Spacecraft Transfer Trajectory Design Exploiting Resonant Orbits in Multi-Body Environments*. Ph.D. Dissertation, Purdue University, West Lafayette, Indiana, 2013.

[9] T. Pavlak, *Mission Design Applications in the Earth-Moon System: Transfer Trajectories and Stationkeeping*. M.S. Thesis, Purdue University, West Lafayette, Indiana, 2010.

[10] D. C. Davis, E. M. Zimovan-Spreen, S. T. Scheuerle, , and K. C. Howell, "Debris Avoidance and Phase Change Maneuvers in Near Rectilinear Halo Orbits," *44th Annual AAS Guidance, Navigation, and Control Conference*, Breckenridge, Colorado, February, 2022.

[11] E. Zimovan, "Characteristics and Design Strategies for Near Rectilinear Halo Orbits within the Earth-Moon System," M.S. Thesis, Purdue University, West Lafayette, Indiana, 2017.

[12] R. Broucke, *Periodic Orbits in the Restricted Three-Body Problem with Earth-Moon Masses*. California Institute of Technology, 1968. JPL Technical Report 82-1168.

[13] V. Szebehely and W. H. Jefferys, "Theory of Orbits: The Restricted Problem of Three Bodies," *American Journal of Physics*, 1968, 10.1119/1.1974535.

[14] A. J. Schwaniger, "NASA Technical Note: Trajectories in the Earth-Moon Space with Symmetrical Free Return Properties," *Lunar Flight Study Series*, 1963.

[15] M. Jesick and C. Ocampo, "Automated Generation of Symmetric Lunar Free-Return Trajectories," *Journal of Guidance, Control, and Dynamics*, 2011, 10.2514/1.50550.